Latest Result of the Fermilab Muon $g - 2$ Experiment

Bingzhi Li[a,*]

[a]*Zhejiang Lab, Hangzhou, 311121, China*

[*]*On behalf of the Muon g − 2 Collaboration*

E-mail: bingzhi.li@zhejianglab.com

The Fermilab Muon $g - 2$ Experiment aims to make precise measurements of the anomalous magnetic moment of the muon (a_μ). The previous result was published in 2021 and the experimental result was 3.3 σ larger than the Standard Model (SM) prediction and was in good agreement with the measurement of the Brookhaven Muon $g - 2$ experiment. In the summer of 2023, we released the latest result of a_μ which is measured to 0.21 ppm, with a factor of 2 improvement in the precision from the Run-2 and Run-3 datasets. Combining with the Run-1 and Brookhaven results, the new world average a_μ is measured to 0.19 ppm. In this proceeding, we will present a brief overview of the experiment, the improvements in the Run-2 and Run-3 analysis, and the outlook of the experiment.

---

[*]Speaker

1. Introduction

The precise measurement of the anomalous magnetic moment of the muon is one of the most stringent tests of the Standard Model (SM) of particle physics, and it is extremely sensitive to new physics. The muon is the second generation lepton in the SM. It is about 200 times heavier than the electron and has a very short lifetime of about $2.2\mu s$ [1]. Due to the large mass, it is more sensitive to new physics phenomena compared to the electron. The Muon $g - 2$ experiment measures a_μ in a uniform and strong magnetic field to explore the characteristics of the muon. The magnetic moment ($\vec{\mu}$) and spin ($\vec{S}$) of muon are connected by a dimensionless factor g: $\vec{\mu} = g\frac{e}{2m}\vec{S}$, where e and m are the charge and mass of the muon. The g factor was predicted to be equal to 2 according to Dirac's equation for any particles with spin $\frac{1}{2}$. However, due to the magnetic anomaly, the g factor is slightly larger than 2 at about 0.1% level. The difference between g factor and 2 is the so-called anomalous magnetic moment: $a_\mu = (g - 2)/2$. The latest precision of the theoretical prediction is 0.37ppm [2]. The experimental measurement of a_μ has been performed many times in history. The previous muon $g - 2$ experiment was performed at the Brookhaven National Laboratory (BNL) and found a result 3.7σ larger than the SM prediction [3]. The discrepancy remained a puzzle to the physicists. To further study the anomaly, Fermilab started a new muon $g - 2$ experiment (E989). The first physics result of the Fermilab muon $g - 2$ experiment was published in 2021 using the Run-1 dataset, which is about 6% of the whole statistics. Combined with the BNL result, the world average experimental a_μ was 4.2σ larger than the SM prediction [4]. After two years of analysis for the Run-2 and Run-3 datasets, the Fermilab experiment released the latest result. The new result is consistent with both the Run-1 result, as well as the BNL result. The precision of the experimental a_μ is reduced to 0.19ppm [5]. Other than the Fermilab experiment, the J-PARC designed a new muon $g - 2$ experiment with a completely different method which is now under construction [6]. The J-PARC muon $g - 2$ experiment plans to start data-taking around 2028.

2. Overview of the Muon $g - 2$ Experiment

The bunched proton beam of the muon $g - 2$ experiment comes from an 8 GeV booster with a bunch width of 120ns. The proton beam hits a pion-production Inconel target [7] and produces pion particles. The pions with an energy of 3.11GeV$\pm$5% will be selected [7]. The pions and decay muons are then sent to the Muon Delivery Ring (DR). After several revolutions around the DR, essentially all of the pions will have decayed into muons. Due to the parity violation in electroweak interactions, the polarized decay muon can be selected through its energy. The polarized muon beam will be stored at the storage ring with a radius of 7112mm and a magnetic field of 1.45T. Due to the g factor larger than 2, the cyclotron frequency (ω_c) and spin frequency (ω_s) of the muon are different. The difference between these two frequencies can be used to extract a_μ:

$$\omega_a = \omega_s - \omega_c = \frac{e}{m}(a_\mu B) \tag{1}$$

where ω_a is the anomalous precession frequency, B is the magnetic field that the muon experienced, e and m are the charge and mass of the muon. Thus, to measure a_μ, we need to measure ω_a and the magnetic field. For the magnetic field, the experiment uses the pulsed nuclear magnetic resonance

(NMR) technique and a calibration chain to express the field in terms of the Larmor precession frequency (ω_p) of the shielded protons within the spherical water sample [8].

The storage ring magnetic field of 1.45T is generated using the C-shaped yoke and superconducting coils with a current of around 5200 A. The peak-to-peak variation of the magnetic field is required to be ±25 ppm in the azimuthal direction. To inject into the storage ring, the muon beam must pass through the solid yoke and the main magnetic field. To overcome the strong fringe field, a dedicated superconducting inflector magnet is used to cancel the field in the beam channel and prevent strong deflection. After the injection, the muon beam enters the storage region at 77mm outside the central closed orbit. To shift the orbit of the muon beam, a fast kicker system is used to steer the beam when the injected beam goes through the kicker region and crosses the storage orbit. The plates will carry current and generate a vertical magnetic field to compensate for the 10.8 mrad angle and shift the beam to its stored orbit. The fast kicker is made up of three 1.27m long aluminum plates and located 90 degrees from the inflector [9]. Other than the fast kicker system, the electrostatic quadrupoles (ESQ) system is used to drive the muons toward the central part of the storage region vertically. The ESQ plates are also made of aluminum due to a similar reason like kicker plates to minimize the perturbation to the 1.45T field. The ESQ covers about 43% of the storage ring. Because of the existence of the E-field, the ω_a expression change to the follow:

$$\omega_a = \frac{e}{m}[a_\mu B - (a_\mu - \frac{1}{\gamma^2 - 1})\frac{\beta \times E}{c}] \tag{2}$$

where γ is the Lorentz factor and E is the E-field. To cancel the effect from the ESQ, a magic γ is selected to be 29.3, while the muon momentum (p) is $3.094 GeV/c$. The muons with $p \neq 3.094 GeV/c$ are slightly affected by the E-field and thus will introduce an E-field correction.

The ω_a measurement is based on the parity violation in the weak interaction, which results in the muon spin and the decay positron's momentum being correlated. The decay positrons with high energies are preferred to be emitted along the muon spin direction while the low-energy positrons prefer to be anti-aligned. This will result in a "wiggle" arrival time of these positrons when making an energy threshold cut on high-energy positrons in the electromagnetic calorimeter system. 24 calorimeters around the storage ring measure the energy and time of the decay positrons from the muon decay. Each calorimeter is made up of a 9 by 6 array PbF$_2$ crystals to detect the positrons [10]. Due to the electrostatic field, the magnetic field, and beam dynamics, the beam distribution varies at different locations of the storage ring as a function of time. A straw tracker system is used to measure the muon beam behavior and extract the beam dynamics parameters. Two straw trackers are used in the experiment, located around 180 degrees and 270 degrees from the inflector, respectively [11]. After correcting for the detector effects like pileup and gain, a fit function including beam dynamic correction terms is used to fit the wiggle plot to extract the ω_a. Fig. 1 shows the wiggle plot and the fit result for the Run-3a dataset.

Dedicated NMR probes are designed to measure the magnetic field and ensure the field is highly uniform to satisfy the precision goal for the experiment. Three sub-systems are used to measure the field. (1) The fixed probes are installed at the bottom and top of the vacuum chamber to offer real-time monitoring and measurement of the magnetic field. There are 378 fixed probes at 72 different azimuth positions to continuously track the field drift and offer feedback to maintain the stability of the field as well. (2) A trolley with 17 NMR probes is used as a movable field
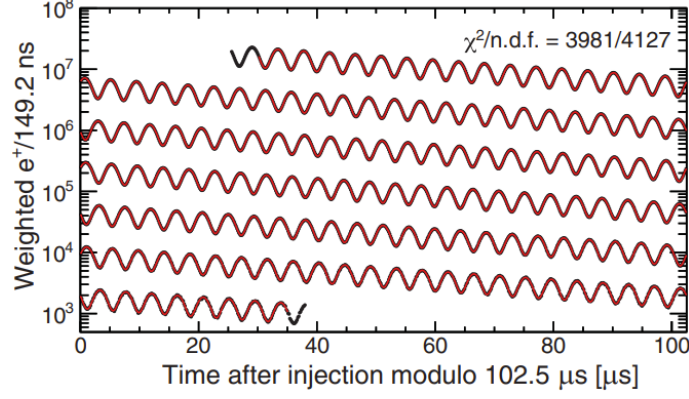
Figure 1: Wiggle plot and the fit result for the Run-3a dataset. The black line is the data while the red line is the fit result. Reproduced from [5].

camera. It scans the field inside the storage ring when the muon beam is off. For a trolley mapping around the ring, each probe measures the field at different azimuth positions about 9,000 times. The mapping is performed every 2 or 3 days to synchronize the fixed probe measurement. (3) The trolley measurements are perturbed by the NMR sample and the electronics. A plunging probe serves as the calibration probe to correct the trolley measurement. During the calibration, the plunging probe and trolley probe would rapidly swap at the same position to measure the same field to extract the calibration constant.

a_μ is extracted from the ratio of the two frequencies ω_a and ω_p:

$$a_\mu = \frac{\omega_a}{\omega_p} \frac{\mu_p}{\mu_e} \frac{m_\mu}{m_e} \frac{g_e}{2} \tag{3}$$

where ω_a is the anomalous precession frequency, ω_p is the shielded proton Larmor precession frequency representing the magnetic field. The experiment measures the first term, and the remaining terms are taken from other individual experiments or calculations with a total uncertainty of 25ppb [4]. The first ratio term can be expressed as:

$$\frac{\omega_a}{\omega_p} = \frac{f_{clock}\omega_a^m(1 + C_{lm} + C_E + C_p + C_{pa} + C_{dd})}{f_{calib}\langle\omega_p(x, y, \phi, Tr) \times M(x, y, \phi)\rangle(1 + B_k + B_q)} \tag{4}$$

where f_{clock} is the hardware blinding to the ω_a measurement. ω_a^m is the spin anomalous precession frequency which is extracted from the wiggle plot fitting. The correction terms C_i in the brackets come from the beam dynamic effects. f_{calib} is the field calibration from the measured Larmor frequency of the proton to the shielded proton frequency at the reference temperature of 34.7 °C. $\langle\omega_p(x, y, \phi, Tr) \times M(x, y, \phi)\rangle$ is the magnetic field weighted by the spatial distribution of the stored muons to represent the field that muon really experienced in the storage ring. The magnetic field measurement also needs to be corrected by two fast magnetic transient effects, B_k arising from the kickers and B_q from the ESQ.

3. Improvements and Result

3.1 Challenges and Improvements

The Run-1 result was statistically limited and also encountered a number of challenges. In the running conditions, we encountered an issue with damaged resistors. Two of the 32 High-Voltage (HV) resistors on the ESQ plates were damaged. This resulted in a changing CBO frequency, which increased the difficulty of the ω_a extraction and involved additional CBO systematic uncertainty. The damaged resistors also result in a large phase acceptance uncertainty, which is the second largest systematic uncertainty source for the Run-1 result. The kicker strength for the Run-1 and Run-2 periods was limited to a lower voltage of 142kV, which resulted in the muon equilibrium orbit being displaced by about 6mm. This leads to a large E-field correction and large beam oscillation amplitude. The hall temperature is not stable during the Run-1 and Run-2 periods; the largest variation can be as large as about 6 degrees, which results in variations in the magnetic field at ppm level. In the systematic studies, due to the limited measurement of the quad transient correction (B_q), the substructure is not measured in Run-1 which results in the largest systematic uncertainty in the Run-1 analysis.

Considering these challenges, many efforts were made to improve the measurement. In the statistics, a factor of 4.7 increase in the number of analyzed positrons reduces the statistic uncertainty from 434ppb to 201ppb. To better store the beam and reduce the beam dynamic effects, the bad resistors were fixed to reduce the beam motion. The Kicker strength was improved during the Run-3 period by upgrading the cables to make a better-centered muon beam to reduce the E-field correction. By updating the hall's air conditioning system and adding thermal insulation to the ring, the temperature can be stable at ±0.5°C for both the magnet yoke and the detector electronics. These efforts reduced the variations of the magnetic field and SiPM gain. Fig. 2 shows some of the improvements from these running conditions upgrades. After fixing the bad resistors and improving the kick voltage, the CBO frequency can be more stable over time. The muon beam can be more centered in the ideal orbit. The hall temperature has been very stable compared to the Run-1 and Run-2 periods.

Other than improving the running conditions to make a better measurement, the analysis method and more systematic runs are further studied. Some new positron reconstruction methods are developed to better count the number of decay positrons, which also reduces the pileup effect. The pileup effect means that when multiple positrons enter the calorimeter in a very short time within the time resolution, these positions would be treated as a single event. The miscounting will result in a ω_a phase shift, leading to an incorrect ω_a frequency. Up to triple pileup events are considered in the Run-2 and Run-3 analyses. With these analysis improvements, the systematic uncertainty of pileup is reduced from 35ppb to 7ppb. To reduce the uncertainty from the field transient effects, which are caused by the vibration from the ESQ plates and the kicker-induced eddy current, more systematical measurements were performed at the ESQ and kicker region: A larger azimuthal range is mapped to better understand the quad transient effects, resulting in a fourfold reduction in uncertainty. An improved magnetometer with reduced noise levels reduces the uncertainty of the kicker transient by a factor of approximately 3. Fig. 3 summarizes the uncertainty comparison between Run-1 and the new results. The total Run-2 and Run-3 systematic uncertainty is about 70ppb which has already achieved the 100ppb systematic uncertainty goal.
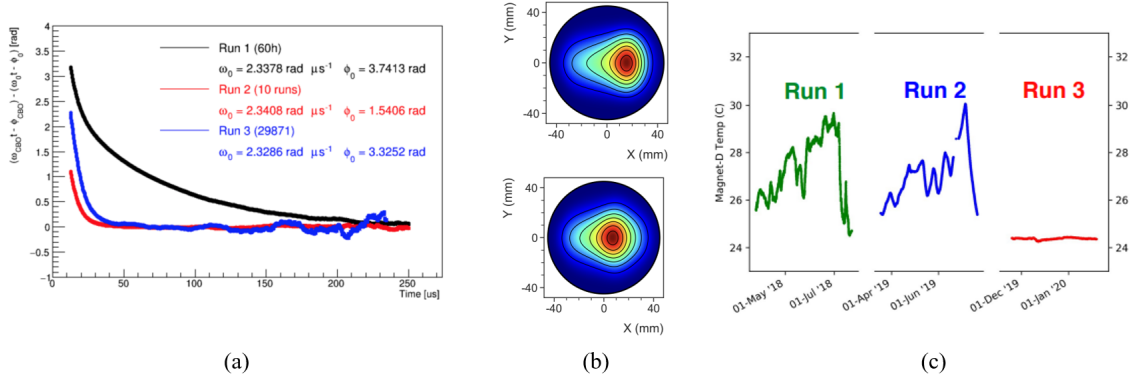
Figure 2: Some improvements from the upgrades of running conditions. (a) plot about the CBO frequencies of some runs from the Run-1 to Run-3 dataset changing over time. (b) plots about the muon distribution in the storage region before (upper) and after (bottom) the kicker upgrades. (c) plot about the hall temperature during the Run-1 to Run-3 periods.
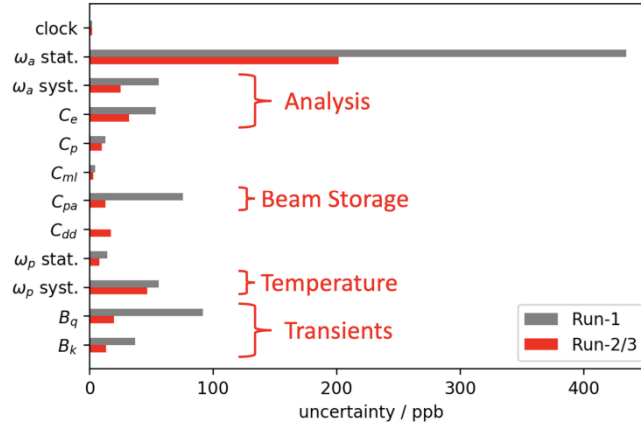
Figure 3: Run-2 and Run-3 systematic uncertainties compared to Run-1

3.2 Result

Like the blinded analysis of the Run-1 dataset, the Run-2 and Run-3 analyses are also fully blinded until the end. The collaboration voted to unblind after all the systematic uncertainties and analyses were finalized. The hardware blind was performed by detuning the hardware clock by non-collaborators, and additional analyzer offsets were set at the software level between different analysis groups. The Run-2 and Run-3 result is shown in Fig. 4, the new result is in good agreement with the Run-1 result with a total uncertainty of 0.21ppm. Combined with the Run-1 result and the BNL result, the uncertainty of the new world average result is further reduced to 0.19ppm. If one makes a simple comparison with the latest theoretical prediction, the discrepancy is 5.1σ. However, some new theoretical results from the lattice QCD method (BMW group [12]) and the dispersive method (CMD3 [13]) reduce the tension between the measurement and the SM prediction, which makes the comparison challenging. Fig. 5 shows the comparison between the different sources of
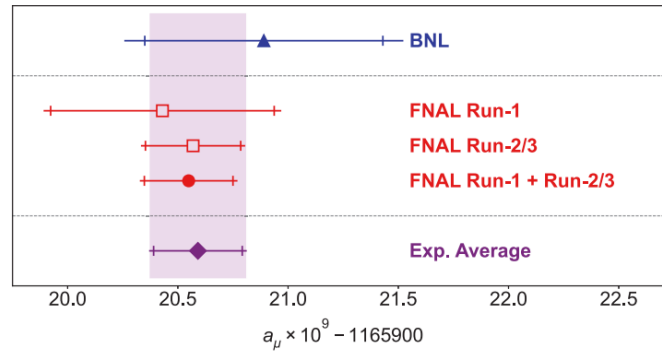
Figure 4: The experimental value of a_μ from BNL result [3], Fermilab Run-1 result [4], Fermilab Run-2 and Run-3 result [5], the combined Fermilab result and the new world average result. The figure is taken from [5]
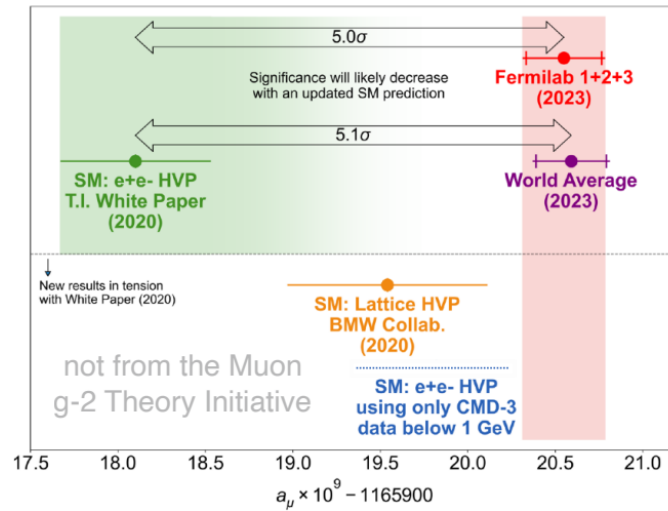
Figure 5: The theory comparison with the experimental measurement. Each data point of the SM value represents a different method of HVP calculation. Taken from the Run-2 and Run-3 released talk.

SM predictions and the experimental result. The theoretical community is making great efforts to improve the calculation as the final experimental results are released around 2025.

4. Conclusion and Outlook

The Fermilab Muon $g − 2$ experiment measured a_μ to 0.21ppm using Run-2 and Run-3 datasets and achieved a factor of 2.2 improvement in both statistical and systematic uncertainties. The major improvements come from the running conditions, more systematic studies, and improved analysis methods. Up to now, the experiment already reached the design goal of systematic uncertainty. Fig. 6 shows that the raw statistics collected in Fermilab compared to the BNL statistics. The Fermilab experiment accumulated a total of 21.9 times the statistics compared to BNL. The physics data-taking was finished in July 2023. The final result is expected to be published in 2025. More systematic studies were performed to better understand beam-related corrections. Some new
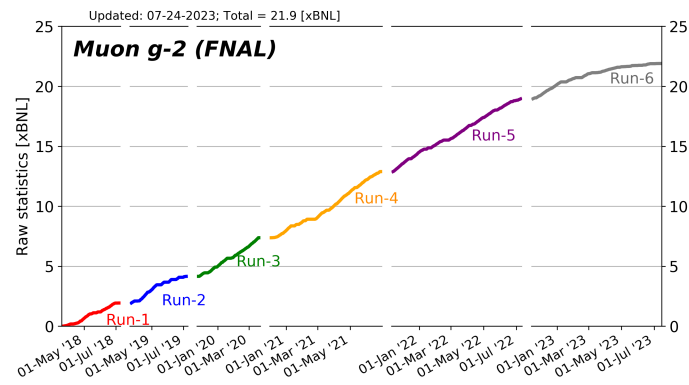
Figure 6: The six-run periods of the Fermilab Muon $g − 2$ experiment. The data-taking was finished on 9th July 2023. The total six physics runs have collected a larger than 21 times statistics more than the BNL experiment which has already reached our design goal.

reconstruction and analysis methods, like re-tracking and machine learning, are studied to further improve the precision. Other analyses like muon EDM, dark matter and Lorentz-CPT violation searches are undergoing.

Acknowledgement

References

[1] R.L. Workman *et al.* [Particle Data Group], Prog. Theor. Exp. Phys. 2022 (2022) 083C01

[2] T. Aoyama *et al.* Phys. Rept. 887 (2020), 1-166.

[3] G. W. Bennett *et al.* [Muon $g − 2$], Phys. Rev. D 73 (2006), 072003.

[4] B. Abi *et al.* [Muon $g − 2$], Phys. Rev. Lett. 126 (2021), 141801.

[5] D. P. Aguillard *et al.* [Muon $g − 2$], Phys. Rev. Lett. 131 (2023), 161802

[6] M. Abe, *et al.* PTEP(2019), 053C02.

[7] J. Grange *et al.* [Muon $g − 2$], arXiv:1501.06858

[8] T. Albahri *et al.* [Muon $g − 2$] Phys. Rev. A 103 (2021), 042208

[9] A.P. Schreckenberger *et al.* Nuclear Instruments and Methods in Physics Research Section A: Accelerators, Spectrometers, Detectors and Associated Equipment 1011 (2021), 165597

[10] K.S. Khaw *et al.* Nucl.Instrum.Meth.A 945 (2019) 162558

[11] B.T. King *et al.* JINST 17 (2022) P02035

[12] S. Borsanyi, *et al.* Nature 593 (2021) 51-55

[13] G. Abbiendi, *et al.* Eur. Phys. J. C 77 (2017) 139

PoS(HQL2023)009